REACTION ZONE STRUCTURE IN SUPRACOMPRESSED DETONATING EXPLOSIVES
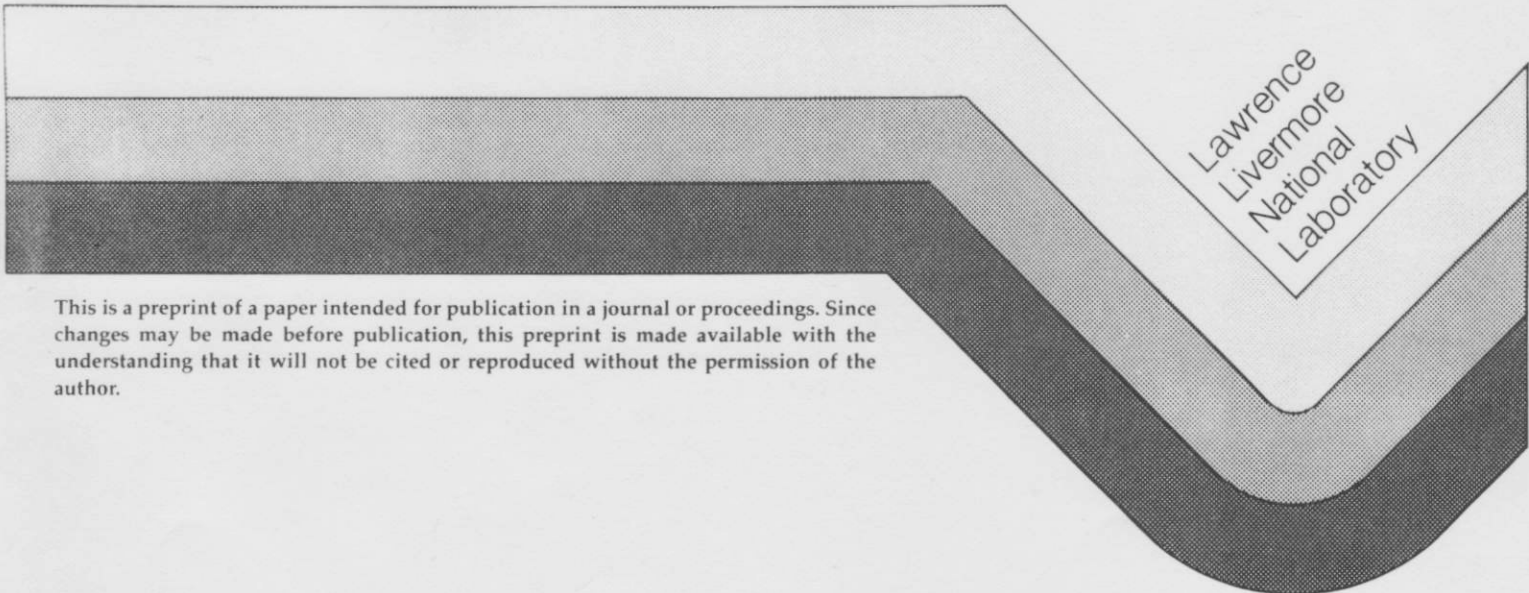
LeRoy G. Green
Craig M. Tarver
David J. Erskine

August 18, 1989

Lawrence Livermore National Laboratory

REACTION ZONE STRUCTURE IN SUPRACOMPRESSED
DETONATING EXPLOSIVES [*]

LeRoy G. Green, Craig M. Tarver, and David J. Erskine
Lawrence Livermore National Laboratory
Livermore, California 94550

Nanosecond time resolved particle velocity histories of supracompressed detonation waves in TNT-, TATB-, and HMX-based explosives are measured using a VISAR laser velocimeter and calculated using the ignition and growth reactive flow hydrodynamic computer code model. The Zeldovich-von Neumann-Doering (ZND) detonation wave structure is observed at pressures more than twice the self-sustaining detonation wave pressure. TNT and TATB exhibited a fast reaction which liberates approximately 80% of the total available exothermicity within 50 ns, followed by a slower reaction which lasts another 100–200 ns. These reaction rates are not strongly dependent on the initial shock pressure. The slower reaction is attributed to diffusion controlled solid carbon coagulation. The ignition and growth model using a ZND type model with a fast reaction preceding a slower reaction to the fully reacted product state accurately calculates the VISAR experimental data for TNT, LX-17, PBX 9404 and RX-26-AF.

INTRODUCTION

In recent years it has become possible to supracompress (overdrive) detonating solid explosives to pressures exceeding their self-sustaining Chapman-Jouguet (CJ) pressures by impacting them with gas-gun accelerated flyer plates at velocities of several millimeters per microsecond. In previous studies, [1-4] subnanosecond time response pins were used to measure shock transit times (shock velocities) in the samples. From the flyer shock Hugoniot and measured velocity, the particle velocity in the supracompressed wave could also be determined. Pressure-volume and shock velocity-particle velocity relationships were determined for several explosives at pressures from just exceeding CJ pressure to approximately 110 GPa. Hydrodynamic computer code calculations showed that the Jones-Wilkins-Lee (JWL) equations of state which accurately calculate product states below the CJ state do not, in general, agree with the supracompression data. Tarver[5] suggested that this discrepancy is due to relatively slow exothermic reactions, such as diffusion controlled solid carbon coagulation into complex structures (graphite, diamond, etc.) which can directly affect the shock front velocity in piston supported waves but only gradually affect the propagation of self-sustaining detonation waves. Supracompression and detonation experiments on PETN, which produces little or no solid carbon in its detonation products, have shown that one JWL equation of state can accurately calculate all of the available data up to 80 GPa.[2,3] A great deal of theoretical and experimental research on the amounts and states of solid carbon produced by detonating under oxidized solid explosives has recently been reported.[6-9] Reactive flow hydrodynamic computer models of the Zeldovich-von Neumann-Doering (ZND) structure of detonation waves in which a fast exothermic reaction is followed by a slower one to the Chapman-Jouguet (CJ) state have accurately simulated a great deal of Fabry-Perot laser interferometric particle velocity history data on detonating HMX-, TATB-, and TNT-based explosives.[10] These calculations also resulted in detonation reaction zone structures similar to those predicted theoretically by Fickett[11] for multireaction sequences.

Although slow carbon condensation reactions appear to explain the shock and particle velocities measured in supracompression experiments, the structures of the reaction zones in these waves could theoretically be quite complex, as illustrated in Fig. 1 of the pressure-specific volume plane. Curve X in Fig. 1 represents the unreacted explosive Hugoniot, curve P1 the incompletely equilibrated reaction products Hugoniot, and curve P2 the completely equilibrated reaction products Hugoniot. Curve P2 is drawn to the right of curve P1 to represent an exothermic process, such as C_1, C_2, C_3, etc. coagulating

FIGURE 1. PRESSURE-SPECIFIC VOLUME RELATIONSHIPS FOR SUPRACOMPRESSED DETONATION WAVES.

The main purposes of this paper are to measure and hydrodynamically model the reaction zones of supracompressed detonation waves in solid explosives containing TNT, TATB, and HMX. The experiments and the reactive flow computer models are briefly described and then the comparison of results is presented.

EXPERIMENTS

The reaction zone structures of supracompressed detonation waves were measured by the laser inteferometric techniques VISAR and Fabry-Perot. The VISAR technique was used on most experiments because it currently has a greater time resolution (approximately 2 ns) and velocity resolution (10–15 m/s) than Fabry-Perot. Plane shock waves were sent through thin explosive samples by accelerating 3 mm thick aluminum plates in the LLNL two-stage light gas gun. The explosive samples were 25 mm in diameter and 2 or 3 mm thick. A 5 mm thick LiF window was attached to the rear of the explosive sample with a 4000 Å gold layer evaporated onto the LiF to provide a specularly reflective surface for the laser interferometer at the explosive/LiF interface. In some experiments, a 0.5 mm thick buffer plate of magnesium alloy AZ31B was placed between the explosive and the LiF window to protect the reflective interface from the three-dimensional irregularities of the leading shock front.[12] Thus the average interface velocity histories between the explosive and LiF or the magnesium and LiF were measured for approximately 500 ns. Table 1 lists the fourteen shots (13 using VISAR and one (BG01) using Fabry-Perot) fired at various flyer plate velocities into TNT, LX-17 (92.5% TATB, 7.5% KelF), PBX 9404, and RX-26-AF (essentially half TATB and half HMX in an estane binder). The details of the experimental techniques (VISAR, pins, fiber optics, data recording, data analysis, etc.) were recently reported in a companion paper.[14]

REACTIVE FLOW MODELING

A reactive flow hydrodynamic computer code model consists of: an unreacted explosive equation of state, a reaction product equation of state, a reaction rate law that governs the chemical conversion of explosive molecules to reaction product molecules, and a set of mixture equations to describe the states attained as the reactions proceed. The unreacted equation of state is normalized to shock Hugoniot and von Neumann spike state detonation data. The reaction product equation of state in normalized to expansion data, such as that obtained in a cylinder test. The reaction rates are inferred from embedded gauge and/or laser interferometric

into long chains of C_{60} or greater. For a CJ self-sustaining detonation wave, the chemical reaction proceeds from the von Neumann spike state S in Fig. 1 along Rayleigh line D to state CJ, where the relatively fast exothermic chain reactions which produce vibrationally excited diatomic and triatomic fluid molecules (N_2, H_2, CO_2, CO, etc.) are completed.[12] Slow exothermic reactions cause the end state of the reaction zone to eventually reach the lower pressure complete equilibration state CJ in Fig. 1. The approach to a steady state CJ detonation for this type of energy release has been discussed by Fickkett.[13] Rayleigh lines 1, 2, and 3 in Fig. 1 represent supracompressed waves supported by pistons at velocities and pressures exceeding the self-sustaining CJ values. Since the entire reaction zone is subsonic at these velocities, the effects of the slow reaction can modify the leading shock front and states along curve P2 should be reached from spike states S_1, S_2, and S_3. As long as the unreacted Hugoniot curves X lies to the left of curves P1 and P2, the measured reaction zone structure will show decreasing particle velocities and pressures such as from state S1 through curves P1 to curve P2 on Rayleigh line 1 in Fig. 1. Should the unreacted Hugoniot be less compressible than the product Hugoniots at very high pressures, measured reaction zone structures may show the effects crossing (or merging) Hugoniots for states such as S_2 and S_3 in Fig. 1.

TABLE 1. TWO-STAGE GUN SUPRACOMPRESSION EXPERIMENTS

	Al Impact		Explosive	Mg (AZ31B)	LiF
Shot	Velocity (km/s)	Explosive	Thickness (mm)	Thickness (mm)	Thickness (mm)
EG06	2.849	TNT (1.645 g/cc)	3	0	5
EG01	2.429 (steel)	TNT	6	0	12.8
EG07	4.167	TNT	3	0	5
EG04	4.455	TNT	3	0	5
EG09	4.725	TNT	2	0.5	5
EG08	6.084	TNT	2	0	5
EG19	3.573	LX-17 (1.903 g/cc)	2	0	5
EG13	3.685	LX-17	2	0.5	5
EG05	4.249	LX-17	2	0	5
EG12	6.191	LX-17	2	0	5
EG14	4.154	PBX9404 (1.843 g/cc)	2	0.5	5
EG15	5.782	PBX 9404	2	0.5	5
EG16	3.910	RX-26-AF(1.836 g/cc)	2	0.5	5
EG17	6.241	RX-26-AF	2	0.5	5

measurements of pressure and/or particle velocity histories. The ignition and growth reactive flow model has been normalized to a great deal of such one- and two-dimensional shock initiation and self-sustaining detonation wave propagation data.[15–20] In this reactive flow formulation, the unreacted and product equations of state are both JWL (i.e., Gruneisen) forms

$$p = Ae^{-R_1V} + Be^{-R_2V} + \frac{\omega C_v T}{V} \qquad (1)$$

where p is pressure, V is relative volume, T is temperature, and A, B, R_1, R_2, ω (the Gruneisen coefficient), and C_v (the average heat capacity) are constants. The ignition and growth reaction rate law is of the form:

$$\frac{\partial F}{\partial t} = I(1-F)^b (\rho/\rho_0 - 1 - a)^x$$

$$+G_1(1-F)^c F^d p^y + G_2 (1-F)^e F^g p^z \qquad (2)$$

where F is the fraction reacted, t is time, ρ_0 is initial density, ρ is current density, p is pressure in Mbars, and I, G_1, G_2, b, x, a, c, d, y, e, g, and z are constants. The first term in equation (2) controls the initial rate of reaction ignited during shock compression and is limited to fraction reacted F ≤ Figmax. The second term in equation (2) is used to simulate the relatively slow growth of hot spot reactions during low pressure shock initiation calculations and the third term is used to rapidly complete the shock to detonation transition in those calculations.[15] However, detonation is a fundamentally

different process from shock initiation and thus must be modeled differently. Recent Fabry-Perot experiments and reactive flow calculations[10] have demonstrated the previously mentioned fast exothermic reaction followed by a slower exothermic reaction. Therefore, for detonation modeling, the second term in equation (2) represents the fast reaction following ignition up to its limiting value F ≤ F_{G1MAX}. The third term is then used to simulate the slow (carbon coagulation) reaction. Table 2 contains the equations of state and reaction rate parameters used for the four explosives studied in this paper. Numbers in parentheses in Table 2 are alternatives used to study the effects of equation of state or reaction rate changes on the simulation of an experiment.

Since the entire supracompression experiment must be accurately modeled with fine zoning (usually 100 or 200 zones per millimeter in the explosive) to obtain nanosecond resolution, the equations of state used for the inert materials are also extremely important. Table 3 lists the Gruneisen form and parameters used for aluminum, steel, magnesium (AZ31B) and LiF in the calculations.

COMPARISON OF EXPERIMENTS AND CALCULATIONS

1) SUPRACOMPRESSED DETONATING TNT

Six experiments (five VISAR and one Fabry-Perot) were done using TNT impacted at various velocities ranging from 2.849 km/s which results in a pressure just

TABLE 2. PARAMETERS FOR IGNITION AND GROWTH CALCULATIONS

Explosive	TNT	LX-17	PBX 9404	RX-26-AF
Unreacted Equations of State				
ρ_0 (g/cc^3)	1.645	1.903	1.843	1.836
A (Mbars)	171.01 (82.57)	778.1 (587.25)(469.76)	9522.	2011.
B (Mbars)	−0.03745 (−0.03609)	−0.05031 (−0.043)(−0.0385)	−0.05944	−0.05204
R_1	9.8(9.0)	11.3	14.1	12.4
R_2	0.98 (0.9)	1.3	1.41	1.24
w	0.5647 (0.5533)	0.8938	0.8867	0.9451
C_v (Mbars/K)	2.7172×10^{-5}	2.48709×10^{-5}	2.781×10^{-5}	2.4063×10^{-5}
T_0(K)	298	298	298	298
Reaction Product Equations of State				
D (mm/µs)	6.930	7.596	8.800	8.239
P_{CJ} (Mbars)	0.180	0.250	0.370 (0.340)	0.325 (0.300)
A (Mbars)	33.94889	43.42773	8.524 (41.8548)	8.018 (31.34582)
B (Mbars)	0.821662	1.94564	0.1802 (1.2553)	0.5264 (1.11739)
R_1	8.3	8.5	4.6 (7.7)	5.0 (7.5)
R_2	2.8	3.28	1.3 (2.4)	2.1 (2.4)
ω	0.6	0.6	0.38 (0.38)	0.34 (0.34)
C_v (Mbars/K)	1×10^{-5}	1×10^{-5}	1×10^{-5}	1×10^{-5}
E_0 (Mbar-cc/ccg)	0.058	0.07	0.102	0.085
Reaction Rate Parameters				
I (µs^{-1})	50.0	4.0×10^6	7.43×10^{11}	14.0
b	0.667	0.667	0.667	0.667
a	0.0	0.22	0.0	0.0
x	4.0	7.0	20.0	4.0
G_1 (Mbars^{-y} µs^{-1})	360.0	48.0	3.1	488.0
c	1.00	0.111	0.667	0.667
d	0.667	0.111	0.667	0.667
y	1.2	1.0	0.111	0.333
G_2 (Mbars^{-z} µs^{-1})	—	500.0	1.0	2.0
e	—	1.0	400.0	500.0
g	—	1.0	0.333	0.222
z	—	3.0	1.0	0.667
Figmax	0.03	0.0232 (0.5)	2.0	3.0
F_{G1MAX}	1.0	0.85	0.3	0.05
			0.5	0.5

above CJ, to 6.084 km/s, which results in a pressure more than twice CJ. The ignition and growth reactive flow model parameters for TNT in Table 2 provide good simulations of Fabry-Perot[10] and ORVIS[18] particle velocity histories measured on self-sustaining detonation waves. The reaction product equation of state for TNT in Table 2 has a lower CJ pressure (18 GPa) than is normally used (19–21 GPa) so that the overall cylinder test energy plus the previously measured supracompression states[21]

can be accurately calculated. Figure 2 shows the experimental VISAR record for the lowest velocity shot EG06 plus the ignition and growth reactive flow calculation. The measured peak velocity is very accurately simulated by the calculation which assumes that only 3% of the reaction occurs promptly during shock compression (Figmax = 0.03 in Table 2) to the state predicted by the unreacted Hugoniot based on R_1 = 9.8 and R_2 = 0.98 that was normalized to von Neumann

TABLE 3. GRUNEISEN EQUATIONS OF STATE FOR INERT MATERIALS

$$p = \rho_0 c^2 \mu \left[1 + (1 - \gamma_0 / 2)\, \mu - a/2\, \mu^2\right] / \left[a - (s-1)\, \mu\right] + (\gamma_0 + a\mu)\, E$$

where p is pressure, ρ_0 is density, c is the intercept of the shock velocity-particle velocity curve, S is the slope of the shock velocity-particle velocity curve $\mu_s = c + s_{up}$, γ_0 is the Gruneisen coefficient, a is the first order volume correction to γ_0, and μ is the relative compression.

Material	ρ_0 (g/cm^3)	c (mm/μs)	S	γ_0	a
Aluminum	2.713	5.24	1.400	1.97	0.48
Steel	7.90	4.57	1.490	1.93	0.5
Magnesium (AX31B)	1.78	4.52	1.242	1.54	0.33
LiF	2.638	5.15	1.350	1.69	0.34

spike states for self-sustaining detonation waves. Figure 2 clearly demonstrates that approximately 80% of the chemical energy is released in the first 60–70 ns while the remaining 20% of the energy is released over the next 70–80 ns or more. The reaction rates listed for TNT in Table 2 simulate this experiment very closely, although the reaction product equation of state predicts a final particle velocity that is 1.5% lower than experiment. Other product JWL equations of state (particularly those with 19–20 GPa CJ pressures) predict this final velocity exactly, but do not calculate correct final velocities at higher pressures. The product JWL in Table 2 is one of the best overall fits to all of the available detonation and supracompression final particle velocity data for TNT.

Figure 3 shows the Fabry-Perot record from shot BG01 which lasted approximately 1800 ns. Also shown in Fig. 3 is the reactive flow calculation which closely agrees with the measured initial velocity and reaction zone structure and then lies near the lowest velocities of the noisy Fabry-Perot record for times of 100–1300 ns. The calculated arrival time of the reflected shock from the steel flyer plate-explosive products interface at ~1300 ns is ~150 ns earlier than the measured arrival at 1450 ns. This experimental arrival time can in principle be used to determine the average sound velocity in the supracompressed products. Figures 2 and 3 also demonstrate the agreement between the VISAR and Fabry-Perot techniques and the usefulness of VISAR for accuracy over the first 500 ns and of Fabry-Perot for obtaining longer records.

Figure 4 contains the VISAR record from shot EG07 in which the aluminum impacted TNT at 4.167 km/s and the corresponding reactive flow calculation. Again the spike state and reaction zone profile to 140 ns are accurately simulated. For this case the calculated final particle velocity is high by 1% or less. Figure 5 shows the

VISAR record and calculation for shot EG04 which had a slightly higher flyer velocity than shot EG07. This experimental record lasted only 200 ns and contained an unusual increase in particle velocity from 60 to 140 ns. The calculated spike velocity and final product velocity agree excellently with experiment but the calculated reaction zone width appears to be too narrow.

The TNT VISAR records imply that the overall reaction zone length in TNT does not decrease with increasing pressure, while the reactive flow model does
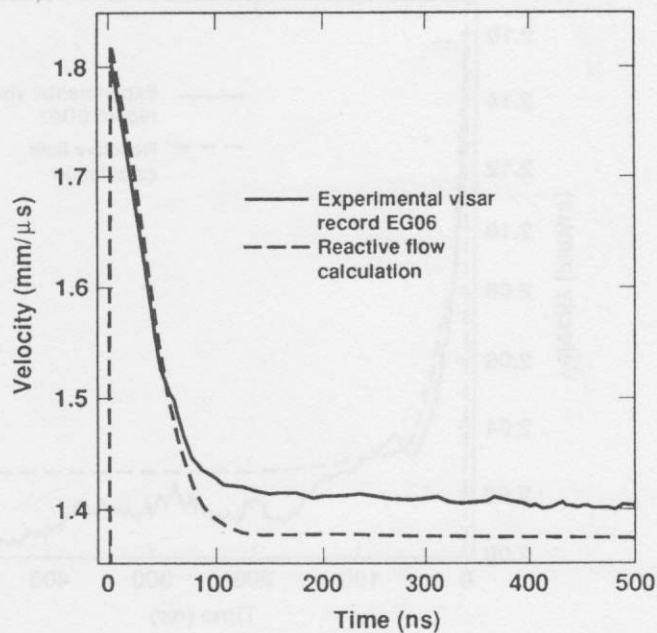

FIGURE 2. TNT SUPRACOMPRESSED EXPERIMENT EG01 ALUMINUM FLYER IMPACT VELOCITY = 2.849 KM/S.
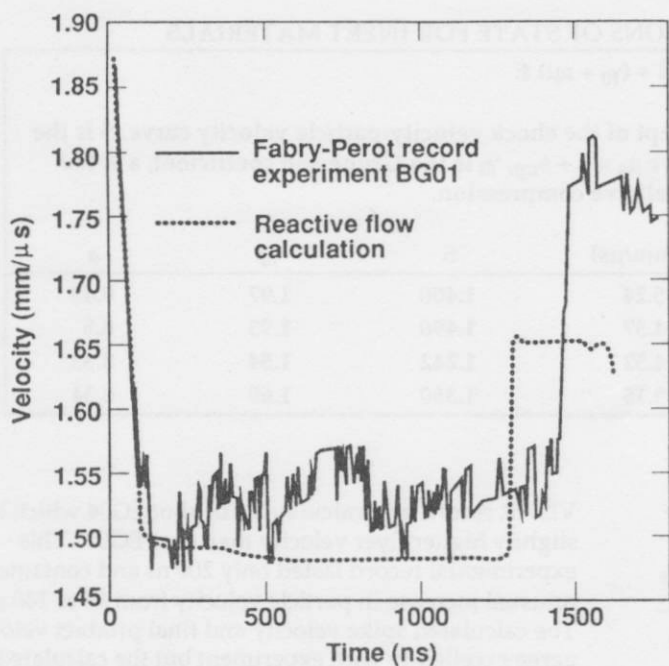
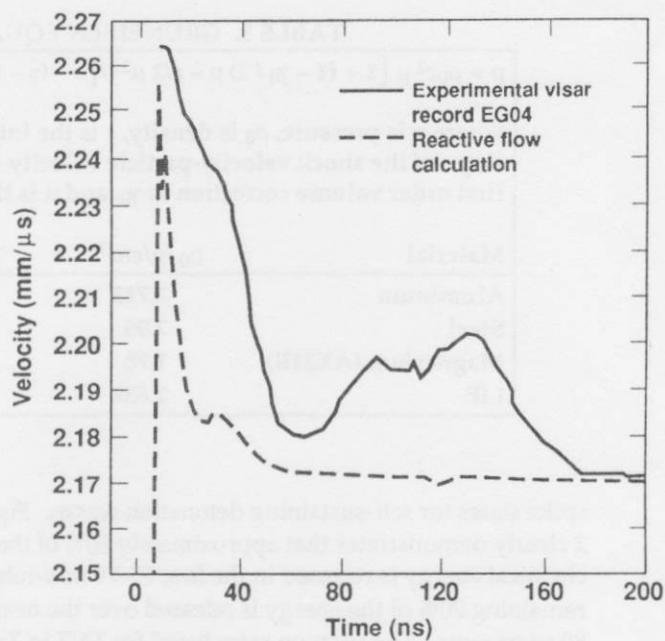FIGURE 3. TNT SUPRACOMPRESSION EXPERIMENT BG01 (FABRY-PEROT) STEEL FLYER IMPACT VELOCITY = 2.429 KM/S.

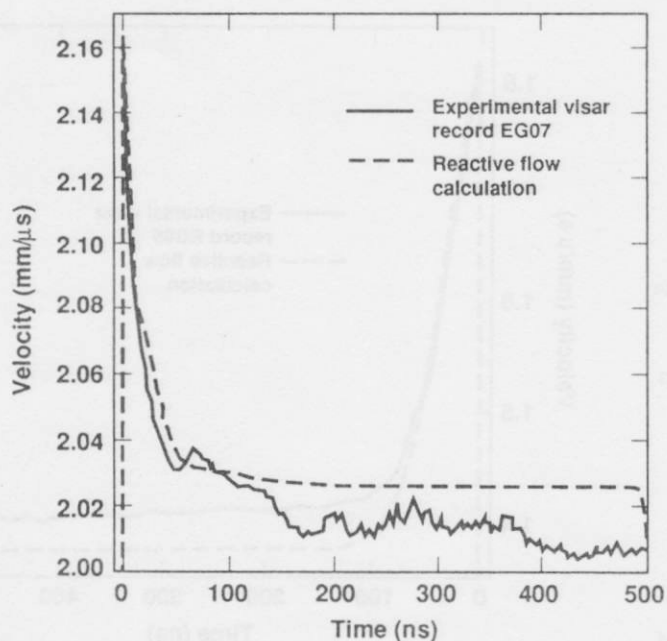FIGURE 4. TNT SUPRACOMPRESSION EXPERIMENT EG07 ALUMINUM FLYER IMPACT VELOCITY = 4.167 KM/S.

FIGURE 5. TNT SUPRACOMPRESSION EXPERIMENT EG04 ALUMINUM FLYER IMPACT VELOCITY = 4.455 KM/S.

predict faster reactions at higher pressures by using an exponent of 1.2 in the pressure dependent second term in equation (2).

Figure 6 contains the VISAR record for shot EG09 which included 0.5 mm of magnesium alloy between the TNT and LiF. Also shown in Fig. 6 are two reactive flow calculations: one used the normal $R_1 = 9.8$, $R_2 = 0.98$ unreacted Hugoniot and the other used a more compressible $R_1 = 9.0$, $R_2 = 0.9$ unreacted Hugoniot which results in a higher spike velocity. The calculated TNT reaction is complete in 80 ns at this input pressure but both calculations are approximately 2% lower than the experimental record, which contains three distinct regions of constant particle velocity lasting over 100 ns.

Figure 7 shows the VISAR record for the highest pressure TNT experiment and two reactive flow calculations with the $R_1 = 9.8$ and $R_1 = 9.0$ unreacted equations of state listed Table 2. Although this VISAR record lasts only 80 ns, it does show a maximum in particle velocity not at the shock front but 20 ns later. This VISAR record is very similar to state S3 of Fig. 1 in which the unreacted Hugoniot X and complete equilibrium Hugoniot P2 lie to the right of the partially reacted Hugoniot P1. The $R_1 = 9.8$ unreacted equation of state spike state is quite low at these extremely high pressures, and the more compressible $R_1 = 9.0$ unreacted
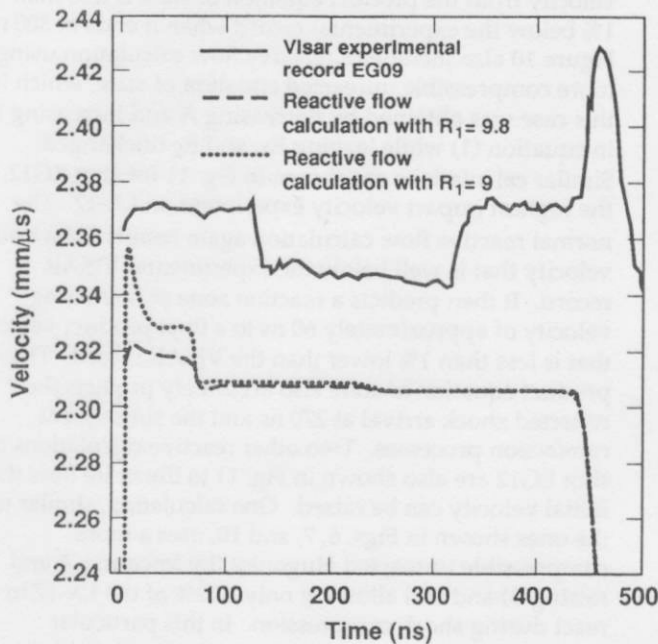
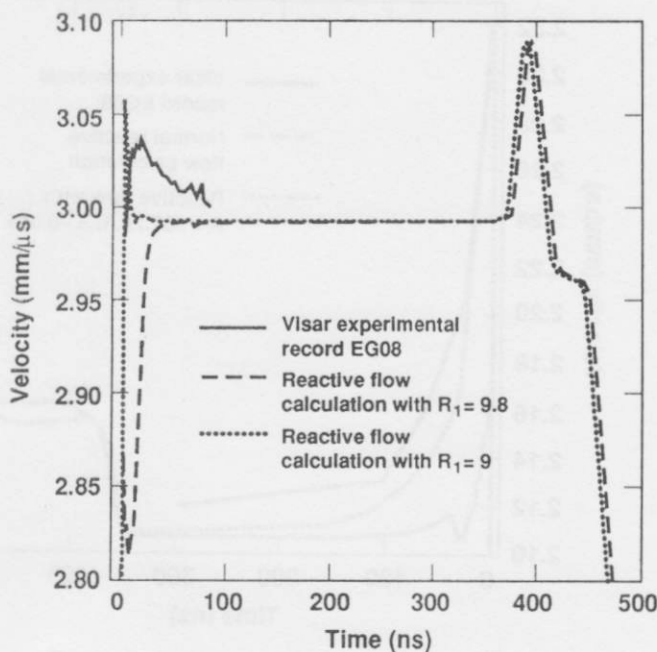FIGURE 6. TNT SUPRACOMPRESSION EXPERIMENT EG09 ALUMINUM FLYER IMPACT VELOCITY = 4.725 KM/S.

FIGURE 7. TNT SUPRACOMPRESSION EXPERIMENT EG08 ALUMINUM FLYER IMPACT VELOCITY = 6.084 KM/S.

equation of state spike state is slightly high. The predicted time for complete reaction of 60 ns is too fast but the product equation of state predicts the correct final particle velocity.

An overall comparison of the six experiments and the various reactive flow calculations for TNT yields the results that the unreacted equation of state from detonation experiments is not compressible enough at very high pressures, the experimental reaction rates are less dependent upon pressure than the model assumes, and that the product equation of state, while not perfect, agrees on the average with the experimentally determined final particle velocities.

2) SUPRACOMPRESSED DETONATING LX-17

As for TNT, the reaction product equation of state listed for LX-17 in Table 2 has a lower CJ pressure (25 GPa) than is normally used (27.5–30 GPa) to match the available supracompression data[1] plus the cylinder test energy. Both the TNT and LX-17 product equation of state use higher values of R_1, R_2 and ω than older JWL cylinder test fits to provide better descriptions of the high pressure (>10 GPa) regime while still matching the overall energy delivered in the cylinder test. The unreacted LX-17 equation of state and reaction rate parameters in Table 2 yield good agreement with self-sustaining detonation reaction zone measurements.[10] Figure 8 contains the VISAR record from shot EG19, the lowest impact velocity experiment on LX-17, and the corresponding reactive flow calculation. The calculated spike and reaction rate agree closely with the VISAR record and, as in TNT, approximately 75% of the reaction occurs in the first 50–60 ns, while the remainder takes at least 200 additional ns. The product equation of state overestimates the final velocity by 1.5–2% but does correctly calculate the arrival of the shock reflected from the aluminum piston-LX-17 interface back at the LX-17-LiF interface. Figure 9 shows the VISAR experimental record from shot EG13, which had a slightly higher impact velocity and a 0.5 mm magnesium alloy buffer, plus the corresponding calculation. The magnesium buffer again adds a great deal of structure to the experimental record that is not as yet totally understood. The calculated peak pressure is high and the velocity history for the 100 ns seems to have a different shape than the VISAR record, but the calculation is generally less than 1% high from 40 to 400 ns.

At higher impact pressures, the LX-17 unreacted equation of state is stiffer than the VISAR records imply, as shown in Fig. 10 for shot EG05. The calculated spike is considerably lower than the VISAR record and causes the whole velocity history to be low, although the final
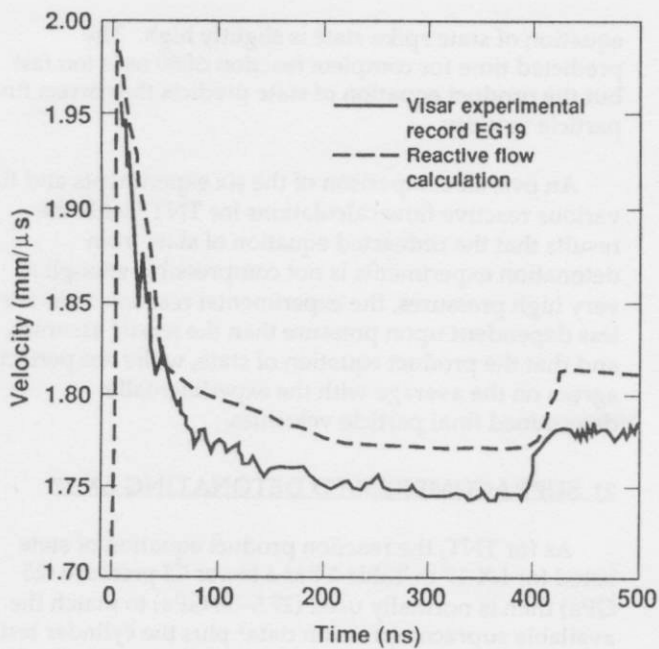
FIGURE 8. LX-17 SUPRACOMPRESSION
EXPERIMENT EG19 ALUMINUM FLYER IMPACT
VELOCITY = 3.573 KM/S.

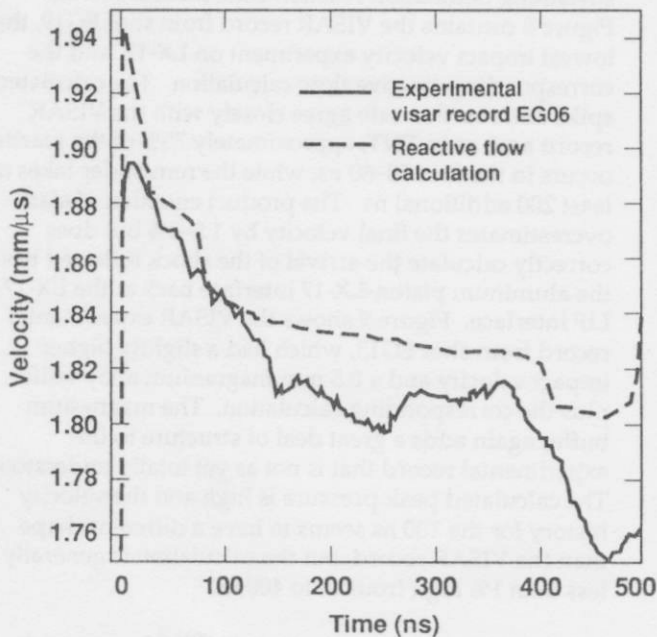FIGURE 9. LX-17 SUPRACOMPRESSION
EXPERIMENT EG13 ALUMINUM FLYER IMPACT
VELOCITY = 3.685 KM/S.

velocity from the product equation of state is less than
1% below the experimental record when it ends at 300 ns.
Figure 10 also includes a reactive flow calculation using a
more compressible unreacted equation of state, which in
this case was obtained by decreasing A and increasing B
in equation (1) while leaving R_1, and R_2 unchanged.
Similar calculations are shown in Fig. 11 for shot EG12,
the highest impact velocity experiment on LX-17. The
normal reactive flow calculation again results in an initial
velocity that is well below the experimental VISAR
record. It then predicts a reaction zone of increasing
velocity of approximately 60 ns to a final product velocity
that is less than 1% lower than the VISAR record. The
product equation of state also accurately predicts the
reflected shock arrival at 270 ns and the subsequent
rarefaction processes. Two other reactive calculations of
shot EG12 are also shown in Fig. 11 to illustrate how the
initial velocity can be raised. One calculation, similar to
the ones shown in Figs. 6, 7, and 10, uses a more
compressible unreacted Hugoniot (by lowering A and
raising B) and still allowing only 2.32% of the LX-17 to
react during shock compression. In this particular
calculation, the reaction rates and mixture algorithm
create a minimum in particle velocity at approximately 15
ns, although the spike and final product states are close
to the VISAR record, which is essentially flat or slightly
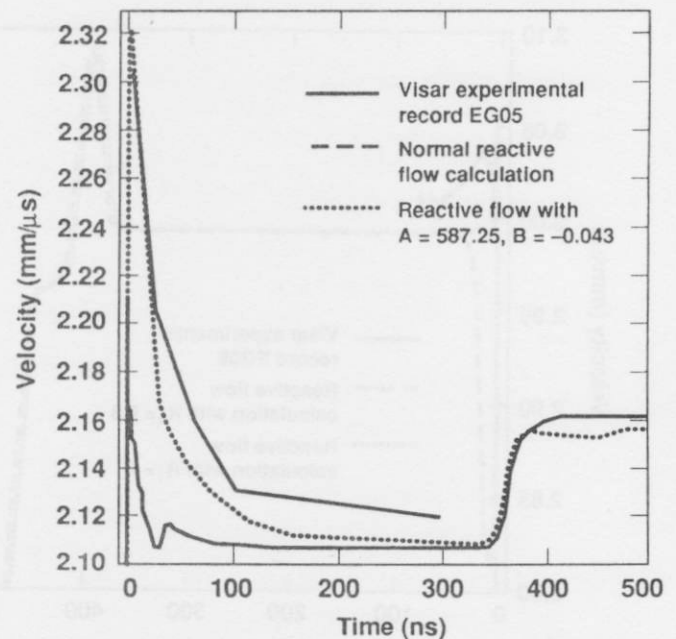increasing for 270 ns. The other calculation allows 50% of

FIGURE 10. LX-17 SUPRACOMPRESSION
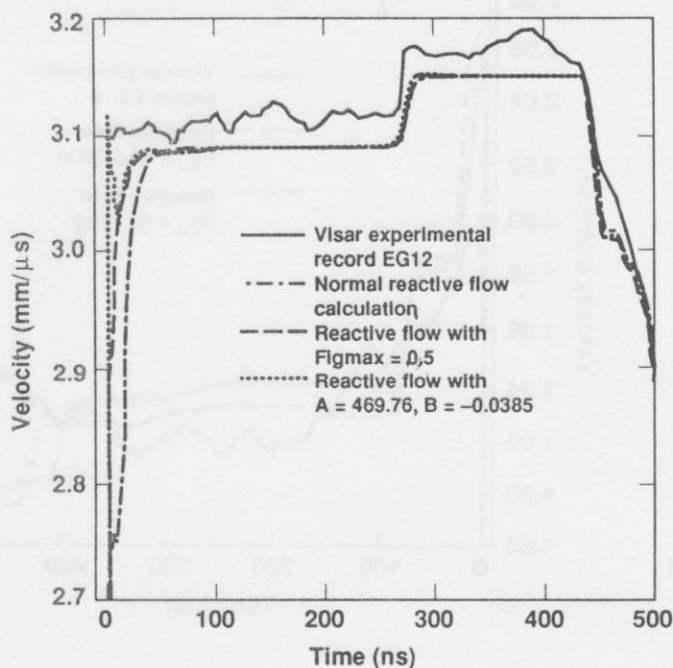EXPERIMENT EG05 ALUMINUM FLYER IMPACT
VELOCITY = 4.249 KM/S.

FIGURE 11. LX-17 SUPRACOMPRESSION
EXPERIMENT EG12 ALUMINUM FLYER IMPACT
VELOCITY = 6.191 KM/S.

FIGURE 12. PBX 9404 SUPRACOMPRESSION
EXPERIMENT EG14 ALUMINUM FLYER IMPACT
VELOCITY = 4.154 KM/S.

the LX-17 to react during shock compression which raises the initial velocity approximately half way to the reaction product equation of state. It is not yet known how much chemical reaction can actually occur within 2 ns (the VISAR time resolution) of the passage of the multidimensional leading shock front as a function of impact pressure. Obviously, if all of the LX-17 had reacted in less than 2 ns in shot EG12, the VISAR record would be flat. However, this is considered unlikely since the three other supracompressed LX-17 VISAR records exhibit reaction zones not much shorter than those measured at detonation (250–300 ns) and since the non-equilibrium ZND model for condensed explosives[12] predicts finite reaction times even at these extreme shock pressures and temperatures.

3) SUPRACOMPRESSED DETONATING PBX 9404

Two shots were fired using PBX 9404, shot EG14 being slightly above the CJ pressure and shot EG15 at a much higher velocity. Due to the complex three-dimensional structure of the HMX detonation wave front, 0.5 mm of magnesium had to be used to protect the LiF crystal. Thus the main reaction zone structure, which is only 20–30 ns for detonating PBX 9404,[10] is obsured in these experiments. Figure 12 shows the VISAR record from shot EG14 and two reactive flow calculations, one
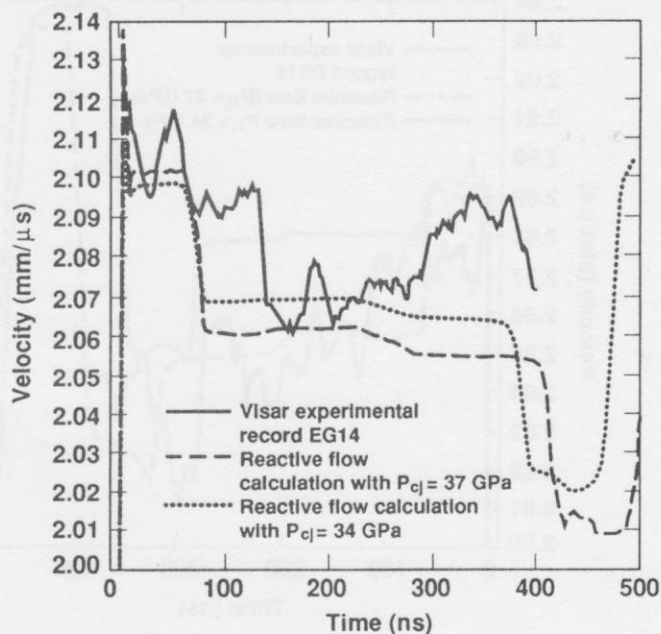
using the standard 37 GPa CJ pressure JWL product equation of state and another using the 34 GPa CJ pressure JWL product equation of state that accurately calculates the shock velocity—particle velocity supracompression data.[1,4] The 34 GPa equation of state was expected to more closely simulate the reaction product state and appears to in Fig. 12, although the difference between the two calculations is not large. The initial calculated velocities agree with the VISAR record in Fig. 12 but the magnesium plate again seems to create a great deal of noise and/or reflected wave structure in the VISAR record. Figure 13 shows the higher velocity shot EG15 and the two reactive flow calculations. Again the calculated initial velocities seem accurate, but the 37 GPa product equation of state agrees more closely with the VISAR record than the 34 GPa calculation, except perhaps in the timing of rarefaction waves and reflected shock waves. More experiments at intermediate pressures are required to resolve this dilemma.

4) SUPRACOMPRESSED DETONATING RX-26-AF

Two shots, one just above CJ conditions and one at very high velocity, were also fired for RX-26-AF, which had previously been modeled[20] using HMX reaction rates for the first 50% reacted and TATB reaction rates for the last 50% reacted. The original JWL product equation
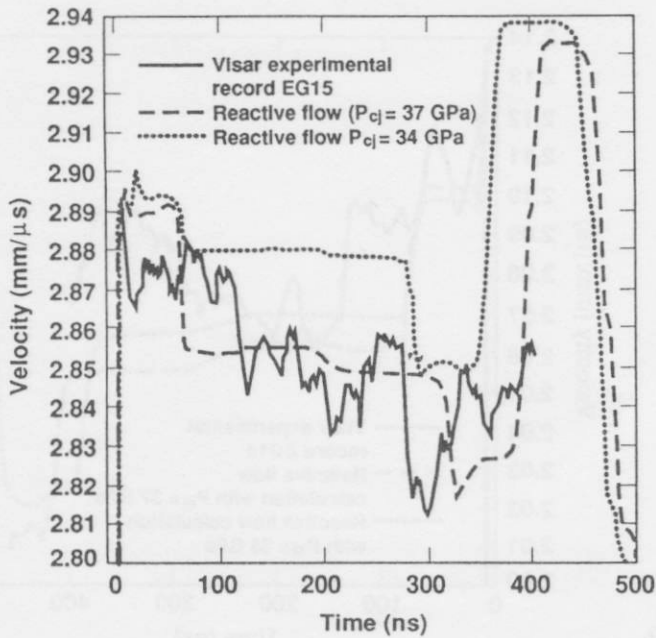
FIGURE 13. PBX 9404 SUPRACOMPRESSION
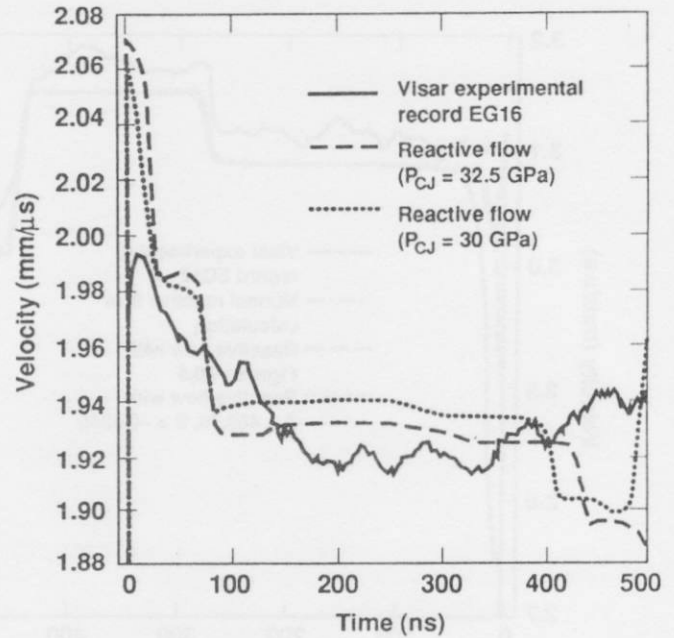EXPERIMENT EG15 ALUMINUM FLYER IMPACT
VELOCITY = 5.782 KM/S.

FIGURE 14. RX-26-AF SUPRACOMPRESSION
EXPERIMENT EG16 ALUMINUM FLYER IMPACT
VELOCITY = 3.910 KM/S.

FIGURE 15. TX-26-AF SUPRACOMPRESSION
EXPERIMENT EG17 ALUMINUM FLYER IMPACT
VELOCITY = 6.241 KM/S.

of state in Table 2 has a CJ pressure of 32.5 GPa, while the
alternate equation of state listed in parentheses in Table 2
has a CJ pressure of 30 GPa and more closely agrees with
previous supracompression shock velocity data.[1] Figure
14 shows the VISAR record for shot EG16 and two
reactive flow calculations, one using the 32.5 GPa CJ
pressure equation of state and one using the 30 GPa CJ
pressure equation of state. The calculated spike is
approximately 3% high, but the RX-26-AF unreacted
equation of state is not normalized to as much Fabry-
Perot data for self-sustaining detonations as are the other
unreacted equations of state. The 32.5 GPa product
equation of state appears to agree slightly better with
most of the VISAR record than the 30 GPa equation of
state. At the higher pressures of shot EG17 in Fig. 15, the
reverse appears to be true with the 30 GPa CJ pressure
equation being closer to experiment, except in the timing
of the reflected shock arrival. More experiments at
intermediate pressures are also required for
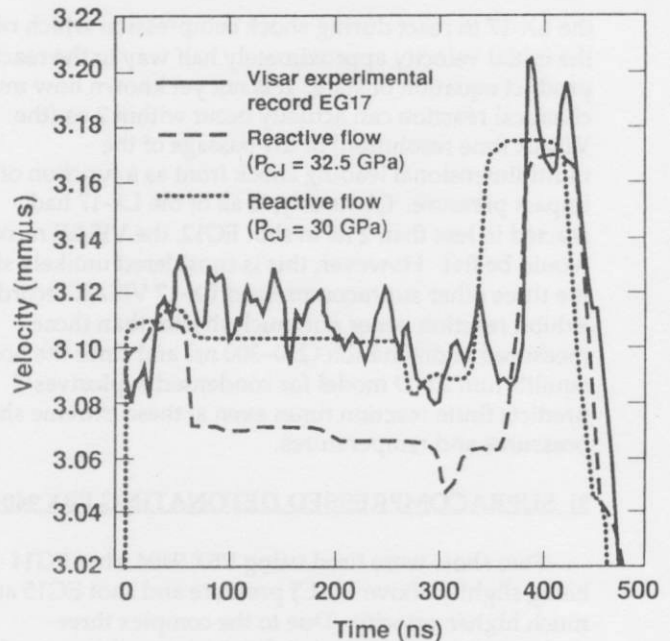understanding supracompressed detonating RX-26-AF.

CONCLUSIONS

The supracompression VISAR experiments and reactive flow calculations presented in this paper have resolved the reaction zone structure of detonating TNT and TATB explosives at several pressures above their normal CJ pressures. Obviously additional VISAR experiments are required to fully study these structures as functions of shock pressure and temperature. The "unreacted" explosive equation of state appears to be more compressible at very high pressures than predicted by the JWL equations of state fitted to low pressure Hugoniot and self-sustaining detonation von Neumann spike data. This problem may be solvable if a more complex equation of state form (perhaps, $U_S = a + bu_p + cu_p^2 + \cdots$) is used to describe the unreacted explosive. However, this issue is complicated by the lack of knowledge of the fraction of the explosive that reacts within the first 2 ns after shock arrival as a function of input pressure. The greater the fraction reacted, the further the initial velocity measurement will be from the true unreacted Hugoniot.

Extrapolation of the self-sustaining detonation reaction rates to these supracompressed states was successful to first order, but the measured reaction rates were less sensitive to pressure than the rates calculated by the pressure dependent ignition and growth model. This is most likely because the supracompressed shock temperatures, which actually control the initial fast reactions, are not much higher than the temperatures reached in various regions of the complex, three-dimensional multishock interaction process that controls self-sustaining detonation. Additionally, the rate of the relatively slow diffusion controlled carbon coagulation process is unlikely to be a strong function of pressure or temperature. More supracompression experiments plus a nanosecond time resolution technique for measuring shock temperatures under these conditions are required for more complete understanding of these global reaction rates.

As demonstrated by the experimental-calculational comparisons, the supracompressed wave structures can be calculated to within 1% in velocity with the current rate laws and equations of state. The reaction product equation of state can also be improved by comparison with more supracompression data and with thermodynamic chemical equilibrium code predictions of these high pressure states. As for the unreacted equation of state, the reaction product equation of state may have to be more complicated than the JWL form currently used. The ability to use nanosecond time resolution techniques, such as VISAR, in the supracompression regime certainly opens many avenues to the understanding of ultra high pressure and temperature reaction rates and equations of state.

REFERENCES

1. L. Green, E. Lee, A. Mitchell, and C. Tarver, Eighth Symposium (International) on Detonation, Naval Surface Weapons Center NSWC MP86-194, 1985, p. 587.

2. L. Green, N. Holmes, and J. King, International Symposium on Pyrotechnics and Explosives, Beijing, China, 1987, p. .

3. L. G. Green, E. L. Lee, D. Breithaupt, and J. Walton, Shock Waves in Condensed Matter—1987 (S.C. Schmidt and N. C. Holmes, Eds.), Elsevier Science Publishers B.V., 1988, p. 507.

4. E. L. Lee, M. Van Thiel, L. G. Green, and A. Mitchell, Shock Waves in Condensed Matter—1983 (J. R. Asay, R. A. Graham, and G. K. Straub, Eds.(Elsevier Science Publishers B.V., 1984, p. 617.

5. C. M. Tarver, On the Difference between Self-Sustaining Converging Detonation Waves and Piston-Supported Overdriven Detonation Waves, UCRL-90714, March 1984, Lawrence Livermore National Laboratory, Livermore, California.

6. J. D. Johnson , "Carbon in Detonations," paper presented at this Symposium.

7. F. H. Ree, and M. Van Thiel, "Dissociation of Nitrogen and EOS of Condensed Carbon: Their Effect on the Detonation Properties of High Explosives," paper presented at this Symposium.

8. N. Roy Greiner, "Chemistry of Detonation Soot: Diamonds, Graphite and Volatiles," paper presented at this Symposium.

9. F. Volk, and F. Schedlbauer, "Detonation Products of Less Sensitive High Explosives Formed Under Different Pressures of Argon and in Vacuum," paper presented at this Symposium.

10. C. M. Tarver, R. D. Breithaupt, and J. W. Kury, International Symposium on Pyrotechnics and Explosives, Beijing, China, 1987, p. 692.

11. W. Fickett, and W. C. Davis, Detonation, University of California Press, Berkeley, 1979, Chapter 5.

12. C. M. Tarver, Combustion and Flame Vol. 46, 1982, p. 157.

13. W. Fickett, Phys. Fluids A Vol. 1, 1989, p. 371.

14. D. J. Erskine, and L. G. Green, "VISAR Measurements of Explosive Reaction Zones," paper presented at the APS Topical Conference on Shock Compression of Condensed Matter, Albuquerque, New Mexico, August 1989.

15. C. M. Tarver, J. O. Hallquist, and L. M. Erickson, Eighth Symposium (International) on Detonation, Naval Surface Weapons Center, NSWC MP 86–194, 1985, p. 951.

16. B. Hayes, and C. M. Tarver, Seventh Symposium (International) on Detonation, Naval Surface Weapons Center, NSWC MP 82–334, 1981, p. 1029.

17. C. M. Tarver, N. L. Parker, H. G. Palmer, B. Hayes, and L. M. Erickson, J. Energetic Materials Vol. 1, 1983, p. 213.

18. S. A. Sheffield, D. D. Blomquist, and C. M. Tarver, J. Chem. Phys. Vol. 80, 1984, p. 3831.

19. K. Bahl, G. Bloom, L. Erickson, R. Lee, C. Tarver, W. Von Holle, and R. Weingart, Eighth Symposium (International) on Detonation, Naval Surface Weapons Center, NSWC MP 86–194, 1985, p. 1045.

20. C. M. Tarver, L. M. Erickson, and N. L. Parker, Shock Waves in Condensed Matter—1983 (J. R. Asay, R. A. Graham, and G. K. Straub, Eds.), Elsevier Science Publishers B.V., 1984, p. 609.

21. J. H. Kineke and C. E. West, Fifth Symposium (International) on Detonation, Office of Naval Research, ACR-184, 1970, p. 533.